Neuron
Article

Regulation of Dendritic Excitability by Activity-Dependent Trafficking of the A-Type K^+ Channel Subunit Kv4.2 in Hippocampal Neurons

Jinhyun Kim,[1,*] Sung-Cherl Jung,[1] Ann M. Clemens,[1] Ronald S. Petralia,[2] and Dax A. Hoffman[1,*]
[1] Molecular Neurophysiology and Biophysics Unit, Laboratory of Cellular and Synaptic Neurophysiology, National Institute of Child Health and Human Development
[2] Section on Neurotransmitter Receptor Biology, National Institute on Deafness and Other Communication Disorders National Institutes of Health, Bethesda, MD 20892, USA
*Correspondence: kimji@mail.nih.gov (J.K.), hoffmand@mail.nih.gov (D.A.H.)
DOI 10.1016/j.neuron.2007.05.026

SUMMARY

Voltage-gated A-type K^+ channel Kv4.2 subunits are highly expressed in the dendrites of hippocampal CA1 neurons. However, little is known about the subcellular distribution and trafficking of Kv4.2-containing channels. Here we provide evidence for activity-dependent trafficking of Kv4.2 in hippocampal spines and dendrites. Live imaging and electrophysiological recordings showed that Kv4.2 internalization is induced rapidly upon glutamate receptor stimulation. Kv4.2 internalization was clathrin mediated and required NMDA receptor activation and Ca^{2+} influx. In dissociated hippocampal neurons, mEPSC amplitude depended on functional Kv4.2 expression level and was enhanced by stimuli that induced Kv4.2 internalization. Long-term potentiation (LTP) induced by brief glycine application resulted in synaptic insertion of GluR1-containing AMPA receptors along with Kv4.2 internalization. We also found evidence of Kv4.2 internalization upon synaptically evoked LTP in CA1 neurons of hippocampal slice cultures. These results present an additional mechanism for synaptic integration and plasticity through the activity-dependent regulation of Kv4.2 channel surface expression.

INTRODUCTION

A number of recent studies investigating the molecular mechanisms of synaptic plasticity have focused on glutamate receptor (AMPAR and NMDAR) trafficking (Bredt and Nicoll, 2003; Groc et al., 2004; Lu et al., 2001; Perez-Otano and Ehlers, 2005; Shi et al., 1999; Snyder et al., 2001). AMPAR subunits in particular display a high degree of mobility, undergoing insertion and removal from the synaptic membrane via endo- and exocytosis, respectively. Changes in the level of synaptic AMPAR expression lead, at least in part, to the degree and direction of synaptic plasticity (Beattie et al., 2000; Brown et al., 2005; Collingridge et al., 2004; Ehlers, 2000; Malinow and Malenka, 2002; Park et al., 2004; Passafaro et al., 2001). It has been shown that rapid insertion of the AMPAR subunit GluR1 mediates an increase in spontaneous miniature excitatory postsynaptic current (mEPSC) amplitude in hippocampal cultured neurons (Lu et al., 2001), while removal of AMPAR subunits GluR1 and GluR2 from the synapses results in LTD of mEPSC amplitudes (Brown et al., 2005). Although these results clearly demonstrate a role for AMPAR trafficking in synaptic plasticity, synaptic events are susceptible to subsequent processing by passive dendritic filtering and dendritic voltage-gated ion channel activity (Cai et al., 2004; Faber et al., 2005; Hoffman et al., 1997; Lipowsky et al., 1996; Magee, 1999; Magee and Johnston, 1995; Ngo-Anh et al., 2005; Ramakers and Storm, 2002). We questioned whether the regulated trafficking of ion channels might also be employed by neurons to control dendritic excitability and synaptic integration.

We focused on the K^+ channel subunit Kv4.2, which underlies the large A-type current found in the dendrites of CA1 pyramidal neurons of the hippocampus. In these neurons, A-type currents have been shown to regulate both sub- and suprathreshold dendritic signals (Cai et al., 2004; Cash and Yuste, 1998; Hoffman et al., 1997; Kim et al., 2005; Ramakers and Storm, 2002). Although Kv4.2 has previously been shown to be enriched in spines (Alonso and Widmer, 1997; Kim et al., 2005), the subcellular trafficking of Kv4.2 has yet to be been investigated. We report here an activity-dependent redistribution of Kv4.2 out of dendritic spines in cultured hippocampal neurons. This redistribution requires NMDAR activation and Ca^{2+} influx and occurs through clathrin-mediated endocytosis. Glycine-induced long-term potentiation (chem-LTP) resulted in concurrent synaptic GluR1 insertion and Kv4.2 internalization. Whole-cell recordings supported these results, showing that endogenous A-type, but not sustained, K^+ currents are reduced after chem-LTP induction. Expression of a Kv4.2 dominant-negative mutant was found to increase mEPSC amplitudes and stimuli that

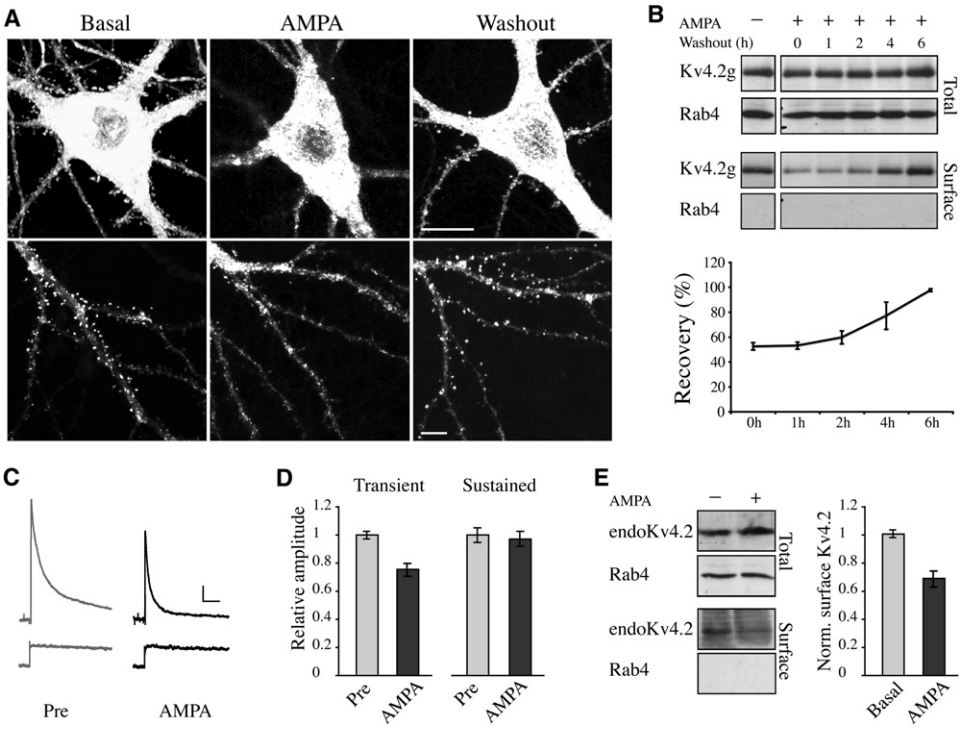

Figure 1. Activity-Dependent Redistribution of Kv4.2 with AMPA Stimulation

(A) AMPA treatment (100 μM) caused a redistribution of Kv4.2g away from synaptic sites and a punctate accumulation of Kv4.2g in the dendritic shaft as well as soma within 15 min. Redistribution of Kv4.2g was reversibly recovered within 6 hr after withdrawal of AMPA (right). Scale bar, 20 μm in top, 8 μm in bottom.

(B) Surface proteins of Kv4.2g-expressing neurons were labeled with NHS-SS-Biotin and probed with anti-GFP. In stimulated neurons the surface level of Kv4.2g was markedly decreased without a significant change in total protein level (100 μM AMPA, 15 min). Time course of surface Kv4.2g recovery showed that internalized Kv4.2g was recruited back into surface membrane within 6 hr after washout of AMPA, consistent with the imaging results. Endogenous Rab4 is shown as cytoplasmic control.

(C) An example of endogenous transient and sustained K^+ currents recorded from the same neuron before (pre) and 5 min after AMPA (50 μM) stimulation. Scale bar, 500 pA, 100 ms. We note here that we likely underestimate the degree of Kv4.2 internalization in our somatic electrophysiological recordings as we only measure K^+ currents located in the soma and proximal dendrites, whereas internalization requires synaptic activity and the majority of endogenous A currents are in distal dendrites.

(D) Normalized K^+ current amplitudes showing that endogenous transient K^+ current amplitudes were significantly decreased upon AMPA stimulation (76% ± 5% of pre, n = 12), while no significant change in sustained K^+ current amplitude was observed. Error bars represent SEM.

(E) Surface level of the endogenous Kv4.2 was determined by biotinylation assay using anti-Kv4.2 in unstimulated or AMPA-stimulated hippocampal slices (100 μM AMPA, 15 min). Consistent with Kv4.2g imaging and biotinylation data, endogenous Kv4.2 is internalized upon AMPA stimulation. Endogenous Rab4 is shown as cytoplasmic control.

induce Kv4.2 internalization resulted in enhanced synaptic currents. Finally, in hippocampal organotypic slice cultures we show that synaptically induced LTP is reduced by hyperpolarization, suggesting that Kv4.2 internalization contributes to LTP. Activity-dependent regulation of Kv4.2 surface expression thus presents a synapse-specific molecular mechanism for the fine-tuning of dendritic signals.

RESULTS

Activity-Dependent Redistribution of Kv4.2

To monitor the subcellular distribution and activity-dependent trafficking of Kv4.2, enhanced green fluorescent protein (EGFP) was attached to the C terminus (Kv4.2g). This construct mimics the somatodendritic expression pattern of endogenous Kv4.2 in hippocampal CA1 pyramidal neurons, with nearly identical biophysical properties (Kim et al., 2005). Using immunogold labeling of endogenous Kv4.2, electron micrographs showed Kv4.2 subunits located in hippocampal CA1 spines, supporting our previous observation of Kv4.2g spine localization (Figure S1 in the Supplemental Data available with this article online). In mature, cultured hippocampal neurons, application of a selective AMPAR agonist (100 μM AMPA, 15 min) caused a redistribution of Kv4.2g out of spines, accumulating in puncta both in the dendritic shaft and soma (Figure 1A). This AMPA-induced redistribution of Kv4.2g was reversible, indicating that the treatment was not excitotoxic and showing that Kv4.2g returns to spines within 6 hr (Figure 1A). Redistribution of Kv4.2g was also observed with KCl (25 mM) depolarization, glutamate (50 μM), and NMDA (20 μM) treatment (Figure S2).

The loss of spine Kv4.2g fluorescence upon stimulation could be due to spine retraction, lateral mobilization of Kv4.2g within the membrane but out of spines, or internalization of Kv4.2g out of the membrane as has been found for AMPARs (Collingridge et al., 2004; Malinow and Malenka, 2002). To test for Kv4.2 internalization, we performed a biotinylation assay to detect surface Kv4.2g levels before and after stimulation. Surface Kv4.2g was markedly decreased in stimulated neurons without a significant change in total protein level (AMPA: 52.5% ± 2.9%, n = 3; total protein: 98.4% ± 2.1%, n = 3; Figure 1B). Again, the stimulation-induced decrease in surface Kv4.2g was almost completely recovered 6 hr after withdrawal of AMPA (normalized surface Kv4.2g level: 53.1% ± 2.7% of basal for 1 hr washout, 59.4% ± 5.1% for 2 hr, 76.4% ± 10.7% for 4 hr, 96.3% ± 1.1% for 6 hr, n = 3; Figure 1B, bottom).

Given the large number of synapses stimulated in these conditions, we were able to directly measure internalization as a decrease in the endogenous whole-cell transient K^+ current from young, uninfected hippocampal neurons (Figures 1C and 1D). After a control recording period, AMPA (50 μM) was applied for 5 min. Endogenous transient K^+ currents measured at +120 mV decreased by 24.5% ± 5.0% after AMPA stimulation (from 2.96 ± 0.19 nA to 2.24 ± 0.19 nA, n = 12, $p < 0.05$, paired Student's t test) without a change in sustained or noninactivating delayed rectifier-type voltage-gated K^+ current amplitudes (0.96 ± 0.05, n = 12, $p > 0.05$, paired Student's t test; Figure 1D). We also noted an increase in the rate of inactivation of the transient K^+ currents after stimulation (from 57.8 ± 7.3 ms to 41.8 ± 8.8 ms, n = 12, $p < 0.05$, paired Student's t test; data not shown). This change in average inactivation rate may indicate targeted internalization of a subset of Kv4.2-containing channels exhibiting slower inactivation (depending on their phosphorylation state or complement of auxiliary β-subunits) (Hoffman and Johnston, 1998; Jerng et al., 2004). Consistent with our imaging and biochemical analysis of Kv4.2g expression, as well as electrophysiological recordings of the endogenous transient K^+ currents, the surface expression level of endogenous Kv4.2 is reduced by AMPA stimulation in acute hippocampal slices as well as in dissociated neurons (normalized surface Kv4.2g level: 67.8% ± 6.1% of basal, n = 4 for slices; Figure 1E; 71.8 8% ± 5.7% of basal, n = 3 for dissociated neurons; data not shown). Thus, the surface expression level of Kv4.2 is regulated by membrane internalization and reinsertion in an activity-dependent manner.

Stimulation triggering Kv4.2g internalization might also lead to changes in synapse number or structure. To determine this, we visualized pre- and postsynaptic elements using antibodies against endogenous Synaptophysin and the primary NMDAR subunit (NR1), respectively (Figure S3). In AMPA-stimulated dendrites, the number of Kv4.2g puncta colabeled with Synaptophysin decreased by approximately 84% (11.9% ± 2.4%, n = 552 puncta from 11 neurons after AMPA versus 75% ± 2.5%, n = 539 puncta from 11 neurons for unstimulated sister cultures, "basal"). Likewise, the number of Kv4.2g puncta colabeled with NR1 was considerably reduced (~82%) upon AMPA stimulation (15.4% ± 3.2%, n = 443 puncta from 12 neurons for AMPA versus 87.7% ± 1.7%, n = 489 puncta from 12 neurons for basal). The number of NR1 clusters per 10 μm of dendrite was unchanged after stimulation (6.54 ± 0.31, n = 24 for AMPA stimulation versus 6.52 ± 0.41, n = 19 for basal). Another spine marker, fluorophore-conjugated phalloidin used to label F-actin, showed similar results (Kv4.2g-positive spines: 17.9% ± 4.5%, n = 500 from 16 neurons for AMPA stimulation versus 89.4% ± 2.2%, n = 1186 from 26 neurons for basal; Figure 2). Kv4.2g therefore appears to undergo activity-induced internalization, without a gross change in synaptic architecture or number.

Clathrin-Mediated Endocytosis of Kv4.2 Is NMDAR and Ca^{2+} Dependent

Preventing synaptic release with tetanus toxin (TeTN) largely eliminated AMPA-induced Kv4.2g redistribution (Kv4.2g-positive spines: 65.6% ± 2.0%, n = 1402 from 27 neurons; Figure 2). In addition, the voltage-gated sodium channel blocker TTX (1 μM) reduced the AMPA-induced redistribution of Kv4.2g but not redistribution induced by KCl depolarization (Kv4.2g-positive spines: 55.7% ± 7.3%, n = 403 from 9 neurons for AMPA + TTX; Figure 2; 10.0% ± 3.0%, n = 264 from 7 neurons for KCl + TTX; Figure S2). These results indicate that, although synaptic release is necessary to trigger Kv4.2g redistribution, AMPAR activation alone is insufficient, suggesting a role for NMDARs. To test for NMDAR dependence, the NMDAR antagonist D,L-APV (100 μM) was applied 15 min prior to AMPA stimulation. NMDAR block largely prevented activity-induced redistribution of Kv4.2g (Kv4.2g-positive spines: 74.9% ± 3.6%, n = 302 from 8 neurons for AMPA + APV; Figure 2; and 59.7% ± 3.3%, n = 270 from 7 neurons for KCl + APV; Figure S2). Consistent with the requirement of synaptic release and NMDAR activation, we found AMPA-induced Kv4.2g redistribution to be blocked by preincubating neurons with the membrane-permeable Ca^{2+} chelator BAPTA-AM (10 μM) (Kv4.2g-positive spines: 78.4% ± 2.6%, n = 544 from 16 neurons for AMPA + BAPTA-AM; Figure 2). Kv4.2g redistribution thus requires NMDAR activation and Ca^{2+} influx.

To estimate the time course of Kv4.2g redistribution, we performed live imaging experiments in cultured hippocampal neurons coexpressing Kv4.2g and the improved red fluorescent protein tdTomato (Shaner et al., 2004). Time-lapse imaging showed that AMPA-driven Kv4.2g redistribution from spines begins rapidly upon stimulation and progresses over a period of about 15 min ($\Delta F/F_0$ of normalized Kv4.2g in spines after 15 min AMPA: −0.25 ± 0.02, n = 192 spines from 9 neurons; Figure 3 and Movie S1). Only a small change in $\Delta F/F_0$ was found in the adjacent dendritic shaft after 15 min AMPA treatment (−0.08 ± 0.03; data not shown). Preincubation with APV almost completely blocked AMPA-induced Kv4.2g fluorescence changes in spines ($\Delta F/F_0$ of normalized Kv4.2g at 15 min

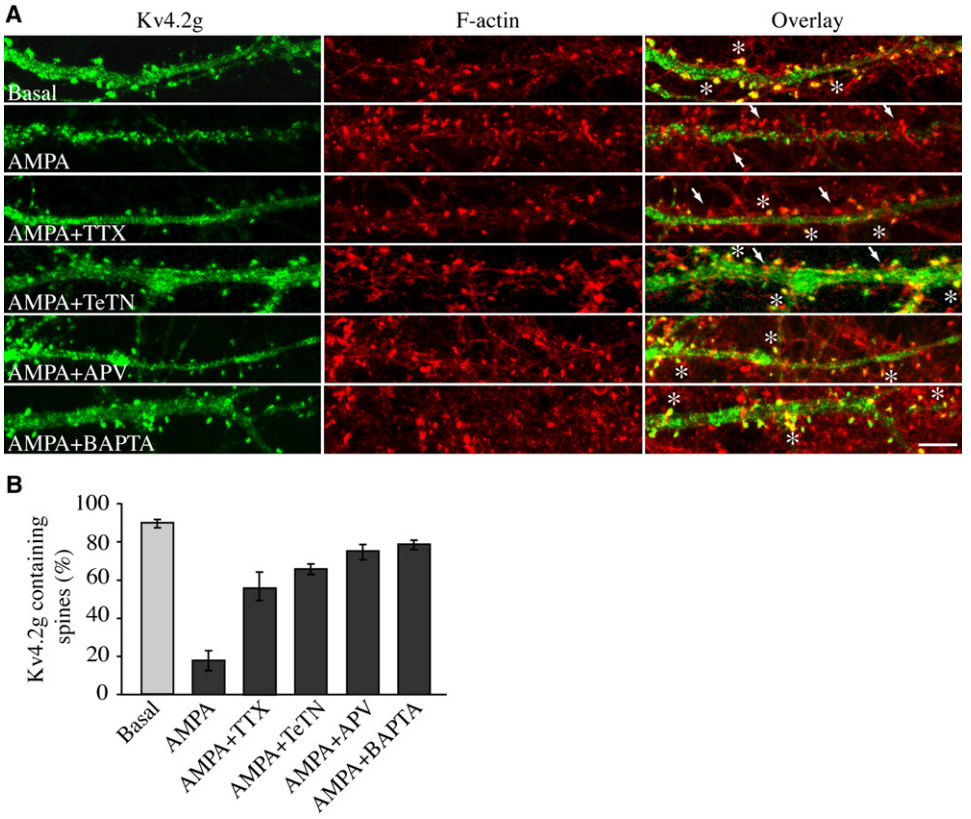

Figure 2. Mechanisms of AMPA-Induced Redistribution of Kv4.2g

(A) Upon 50 μM AMPA (15 min), most F-actin-labeled spines lost Kv4.2g fluorescence. Spines were detected by TRITC-phalloidin labeling of F-actin. AMPA-induced redistribution of Kv4.2g was reduced when cotreated with the voltage-gated Na^+ channel blocker (TTX, 1 μM), Tetanus neurotoxin (TeTN, 20 nM), the NMDAR antagonist D,L-APV (100 μM), or the membrane-permeable Ca^{2+} chelator BAPTA-AM (10 μM), 15 min prior to AMPA stimulation. Asterisks, Examples of Kv4.2g-positive spines; arrows, Kv4.2g-negative spines. Scale bar, 8 μm.

(B) Summarized ratio of the number of Kv4.2g-positive spines to total spines for each treatment. Error bars represent SEM.

time point: −0.05 ± 0.02, n = 100 spines from six APV-treated neurons versus −0.02 ± 0.01, n = 75 spines from nontreated four neurons; Figure 3 and Movie S2; non- or APV-pretreated dendritic shafts: −0.01 ± 0.01; data not shown).

We next addressed the mechanism of Kv4.2g redistribution using a synthetic Dynamin-derived peptide (DYN) to inhibit clathrin-mediated endocytosis by blocking the recruitment of Dynamin to clathrin-coated pits (Damke, 1996; Nong et al., 2003). This peptide has been used previously to show that functional AMPA receptor expression level is controlled by clathrin-dependent receptor internalization (Brebner et al., 2005). Imaging and electrophysiological experiments both show that activity-dependent Kv4.2g redistribution and/or endogenous A current reduction is blocked by the DYN peptide (Figure 4). Preincubation of cultured neurons with membrane-permeable myrs-DYN for 10 min almost completely eliminated AMPA-mediated Kv4.2g redistribution, whereas a scrambled peptide (myrs-scramDYN) had no effect on Kv4.2g redistribution (Kv4.2g-positive spines: 82.3% ± 1.6%, n = 927 from 20 neurons for AMPA + myrs-DYN and 20.0% ± 2.6%, n = 455 from 13 neurons for AMPA + myrs-scramDYN; Figures 4A and 4B). Preventing endocytosis by preincubating neurons in hypertonic media (0.45 M sucrose) also abolished AMPA-induced Kv4.2g redistribution (Kv4.2g-positive spines: 92.1% ± 1.9%, n = 685 from 19 neurons; data not shown). AMPA-driven Kv4.2g redistribution thus occurs through clathrin-mediated endocytosis.

In support of the imaging results, inclusion of membrane-impermeable DYN (but not scramDYN) in the patch pipette in whole-cell recordings prevented the AMPA-induced reduction of endogenous A currents in cultured hippocampal neurons (normalized peak transient current after AMPA stimulation for DYN, 0.91 ± 0.02, $p > 0.05$, paired Student's t test, n = 7; Figures 4C and 4D). In recordings using scramDYN, AMPA again reduced endogenous transient but not sustained K^+ currents (normalized peak transient current after AMPA stimulation for scramDYN, 0.57 ± 0.07, $p < 0.05$, paired Student's t test, n = 4; Figures 4C and 4D).

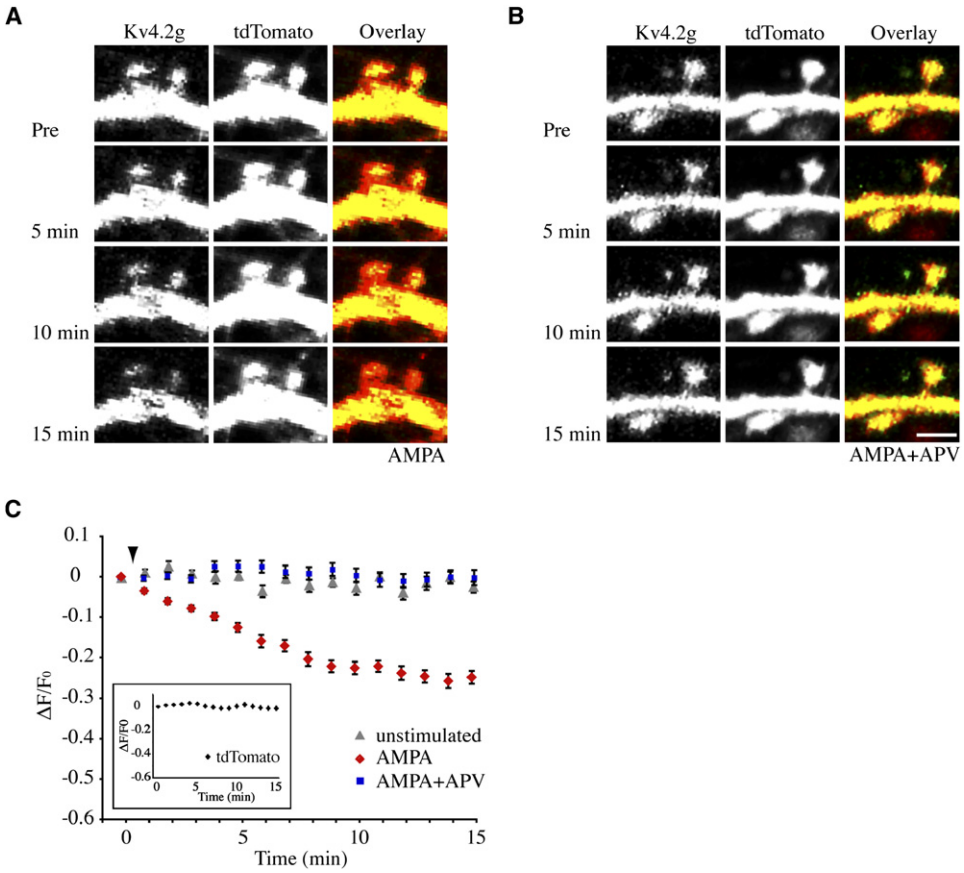

Figure 3. Time-Lapse Images of Kv4.2g Redistribution

(A) Time-lapse images showing Kv4.2g fluorescent intensity decrease upon AMPA (50 μM) stimulation in spines of hippocampal neurons coexpressing Kv4.2g and tdTomato.

(B) Kv4.2g fluorescence intensity was not significantly changed with APV coapplication. Scale bar, 2 μm.

(C) Time course of averaged fractional fluorescent changes ($\Delta F/ F_0$) of Kv4.2g in spines. AMPA stimulation resulted in a progressive decrease of Kv4.2g-specific fluorescent intensity in spines, with no significant change in tdTomato fluorescent intensity (inset). AMPA-mediated decreases in spine Kv4.2g fluorescence intensity were blocked by preapplication of 100 μM APV. Error bars represent SEM.

These experiments revealed a physiological consequence of Kv4.2 internalization: a reduced capacity for neurons to counter membrane depolarization. In these recordings, we monitored the peak AMPA-induced membrane depolarization (see Experimental Procedures) and the time it took to recover after washout. Upon AMPA stimulation, intracellular DYN reduced both peak membrane depolarization and recovery time compared to scramDYN (Figure 4E) and control recordings (no peptide, −36.42 ± 1.69 mV peak depolarization and 305.83 ± 16.01 s for recovery, n = 12). These data show that regulated Kv4.2 trafficking provides a potent mechanism for controlling membrane excitability.

Kv4.2 and GluR1 Are Differentially Redistributed upon AMPA Stimulation

Previous investigations demonstrated AMPAR internalization by a number of different stimuli (synaptic activity, insulin treatment, Ca^{2+} influx, and ligand binding to AMPARs) (Brown et al., 2005; Carroll et al., 1999; Lin et al., 2000; Lissin et al., 1999; Park et al., 2004; Zhou et al., 2001), through distinct endosomal sorting pathways. Ligand binding (i.e., AMPA) induced AMPAR internalization is NMDAR independent (Lin et al., 2000; Lissin et al., 1999), indicating a separate internalization mechanism from our results with Kv4.2. To compare the trafficking of Kv4.2 and AMPARs, Kv4.2g-expressing neurons were stimulated by AMPA (50 μM, 15 min) and subsequently immunostained with anti-GluR1 to detect endogenous AMPARs. AMPA treatment triggered the internalization of both Kv4.2g and GluR1 away from spines into the dendritic shaft (Figure 5). For analysis, Kv4.2g and GluR1 fluorescent signal intensity was plotted for both the dendritic shaft and spines, as illustrated in Figure 5B. Line plots of spine fluorescence indicated almost complete colocalization of Kv4.2g and GluR1 in unstimulated dendritic spines, which was abolished with AMPA stimulation (Figures 5A and 5C). Within the dendritic shaft, after

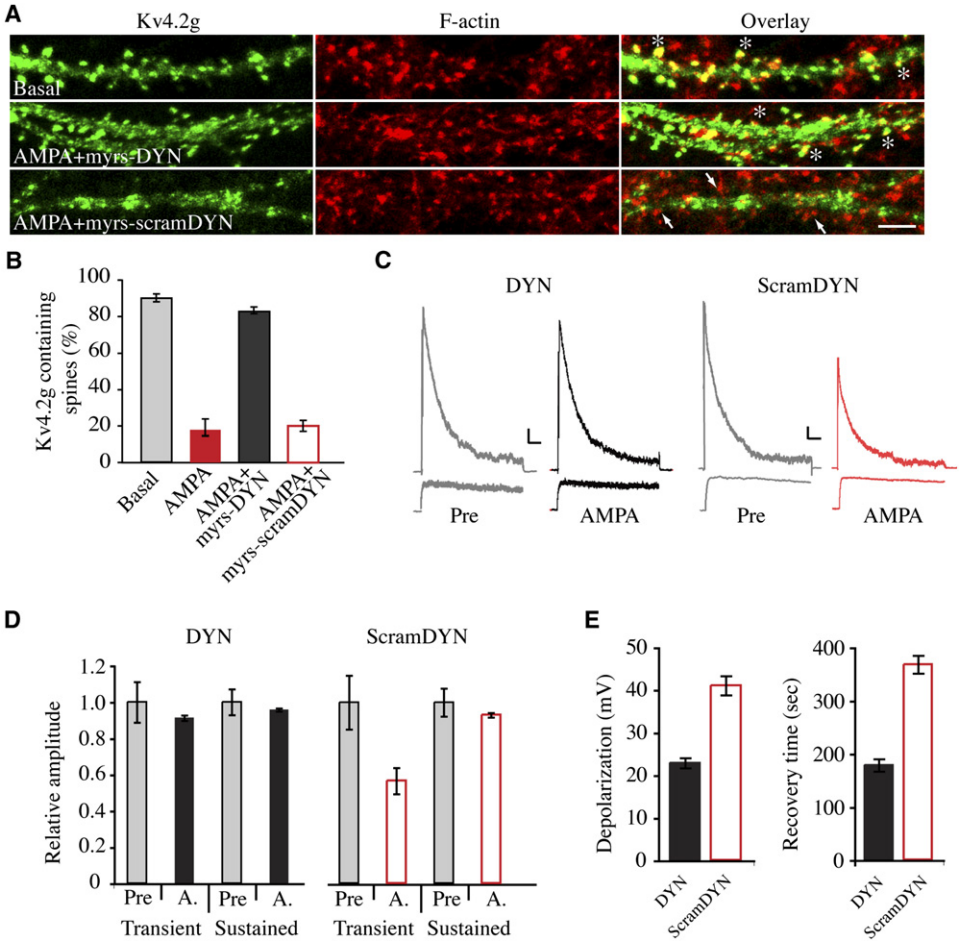

Figure 4. Clathrin-Mediated Endocytosis of Kv4.2 upon AMPA Stimulation

(A and B) Dynamin inhibitory peptide (myrs-DYN, 50 μM), bath-applied 10 min prior to AMPA stimulation (50 μM, 15 min), blocked Kv4.2g internalization. Scrambled dynamin peptide (myrs-scramDYN, 50 μM) was used as a negative control. Asterisks, Kv4.2g-positive spines; arrows, Kv4.2g-negative spines. Scale bar, 8 μm.

(C) An example of endogenous transient and sustained K^+ currents recorded from the same neuron before (pre) and 5 min after AMPA (50 μM) stimulation with DYN (100 μg/ml) or scramDYN (100 μg/ml) included in the patch pipette. Scale bars, 200 pA, 50 ms.

(D) Normalized K^+ current amplitudes showing that AMPA (50 μM, 5 min)-induced decreases of endogenous transient K^+ currents were blocked by DYN but not with scramDYN. No significant change in sustained K^+ current amplitude was observed in either condition. Error bars represent SEM.

(E) DYN but not scramDYN reduced AMPA-mediated membrane depolarization and reduced recovery times compared to control recordings with no intracellular peptide (36.42 ± 1.69 mV peak depolarization and 305.83 ± 16.01 s for recovery, n = 12). Error bars represent SEM. Myristoylated DYN was used in imaging but not electrophysiology experiments. K^+ channels were recorded 3–8 min after recovery from AMPA stimulation.

AMPA stimulation, fluorescent signals from internalized Kv4.2g and GluR1 were nonoverlapping. Coapplication of APV and AMPA resulted in GluR1 but not Kv4.2g redistribution (Figures 5A, 5C, and 5D). These results show that AMPA-dependent internalization of the two channels proceeds through distinct intracellular pathways.

We note that GluR1 internalization during AMPA stimulation would be expected to decrease neuronal excitability. Thus, the reduced depolarization observed upon AMPA stimulation in experiments where internalization is blocked using an inhibitory dynamin peptide (DYN, Figure 4E) may actually reflect an underestimate of the effect of Kv4.2 internalization on membrane excitability.

Kv4.2 Internalization Affects Dendritic Integration of Synaptic Input

To determine if surface Kv4.2 expression affects synaptic integration, we altered the level of functional Kv4.2 by expressing Kv4.2g or the dominant-negative mutant $Kv4.2g^{W362F}$ (Kim et al., 2005; Malin and Nerbonne, 2000) and compared basal mEPSC amplitudes (Figure 6). Whole-cell transient K^+ currents were increased ~2-fold in Kv4.2g-expressing neurons, and decreased ~60% in $Kv4.2g^{W362F}$-expressing neurons compared to control, with no change in the sustained K^+ current amplitude (*transient*: 7.85 ± 0.56 nA, n = 6 for Kv4.2g-expressing versus 3.87 ± 0.46 nA, n = 7 for control and 1.97 ± 0.22 nA,

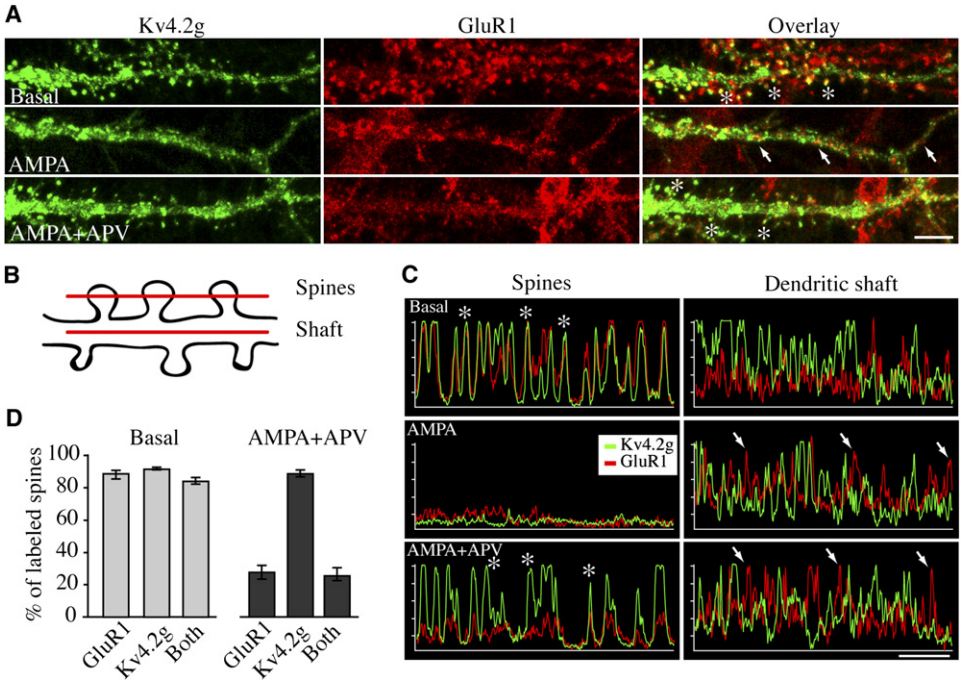

Figure 5. Kv4.2g and GluR1 Differently Redistributed upon AMPA Stimulation

(A) Kv4.2g and GluR1, overlapped in spines in basal conditions, were not colocalized after AMPA stimulation (50 μM, 15 min). APV application resulted in Kv4.2g-only positive spines, indicating distinct internalization pathway of Kv4.2 and GluR1 upon AMPA stimulation. Asterisks, Kv4.2g-positive spines: arrows, Kv4.2g-negative spines. Scale bar, 8 μm.

(B) Illustration of lines used to compare fluorescent intensity in spines and dendritic shaft.

(C) Representative linear plot analysis of Kv4.2g (green) and GluR1 (red) distribution. x axis indicates a length along dendrite, and y axis indicates fluorescent intensity (range 0–255, arbitrary units). In line scans, peaks correspond to spines containing Kv4.2g and/or GluR1 (left), or clusters in dendritic shaft (right). Upon AMPA stimulation, fluorescent peaks of both Kv4.2g and GluR1 were abolished in spines. In APV-treated spines, peaks of Kv4.2g were detected but not those of GluR1. In APV-treated dendritic shafts, peaks of Kv4.2g and GluR1 were not colocalized, once internalized by AMPA. Scale bar, 10 μm.

(D) Summarized number of Kv4.2g- and/or GluR1-containing spines (Kv4.2g-containing spines, 93% ± 2.1%; GluR1-containing, 29.5% ± 4.4%; overlapping, 27% ± 4.3%, n = 417 from 11 neurons for AMPA + APV versus 93% ± 0.8%, 91% ± 2.5%, 86 ± 2%, n = 439 from 8 neurons for basal). Error bars represent SEM.

n = 7 for Kv4.2g^{W362F}, $p < 0.05$, one-way ANOVA; *sustained*: 1.23 ± 0.13 nA, n = 6, 1.19 ± 0.38 nA, n = 6 and 1.56 ± 0.86 nA, n = 7 for Kv4.2g, control, and Kv4.2g^{W362F}, respectively, $p > 0.05$; data not shown) (Kim et al., 2005).

Functional Kv4.2 expression level determined basal mEPSC amplitude (11.7 ± 0.5 pA, n = 31 for control versus 10.8 ± 0.8 pA, n = 17 for Kv4.2g and 17.6 ± 1.5 pA, n = 15 for Kv4.2g^{W362F}, $p < 0.05$, one-way ANOVA; Figures 6A and 6B) and rise time (11.7 ± 0.5 pA, n = 31 for control versus 10.8 ± 0.8 pA, n = 17 for Kv4.2g and 17.6 ± 1.5 pA, n = 15, for Kv4.2g^{W362F}, $p < 0.05$, one-way ANOVA; data not shown). Due to inadequate voltage control of the synapse, synaptic charge is a more accurate measure of synaptic efficacy than amplitude (Barrett and Crill, 1974; Carnevale and Johnston, 1982; Spruston et al., 1993). We found that charge (measured as the total mEPSC area) also depended on the level of functional Kv4.2 (81.7 ± 5.4 pA*ms for control versus 64.1 ± 4.4 pA*ms for Kv4.2g and 117.8 ± 11.0 pA*ms for Kv4.2g^{W362F}, $p < 0.05$, one-way ANOVA; Figure 6B). Figure 6C shows the normalized charge distribution for all recorded mEPSCs. Kv4.2g^{W362F}-expressing neurons displayed a broader charge distribution with a shift toward larger charges compared to control, whereas Kv4.2g-expressing neurons had a more narrow distribution range with a shift toward smaller charges. In control, uninfected neurons, bath application of 4-aminopyridine (4-AP, 7 mM) to block endogenous A-type K^+ channels increased mEPSC charge in three of five neurons tested (Figure 6D, $p < 0.05$, paired Student's t test).

The effect of Kv4.2 on mEPSC amplitudes suggests a mechanism by which active synapses could increase their efficacy by locally decreasing Kv4.2 surface expression. In our imaging experiments, NMDARs were activated through global, AMPA-mediated depolarization and subsequent glutamate release. That TTX did not entirely block Kv4.2 redistribution (Figure 2) suggests that, upon depolarization, spontaneous activity may provide sufficient NMDAR activation to induce Kv4.2 internalization. To test this possibility, we monitored mEPSCs before and

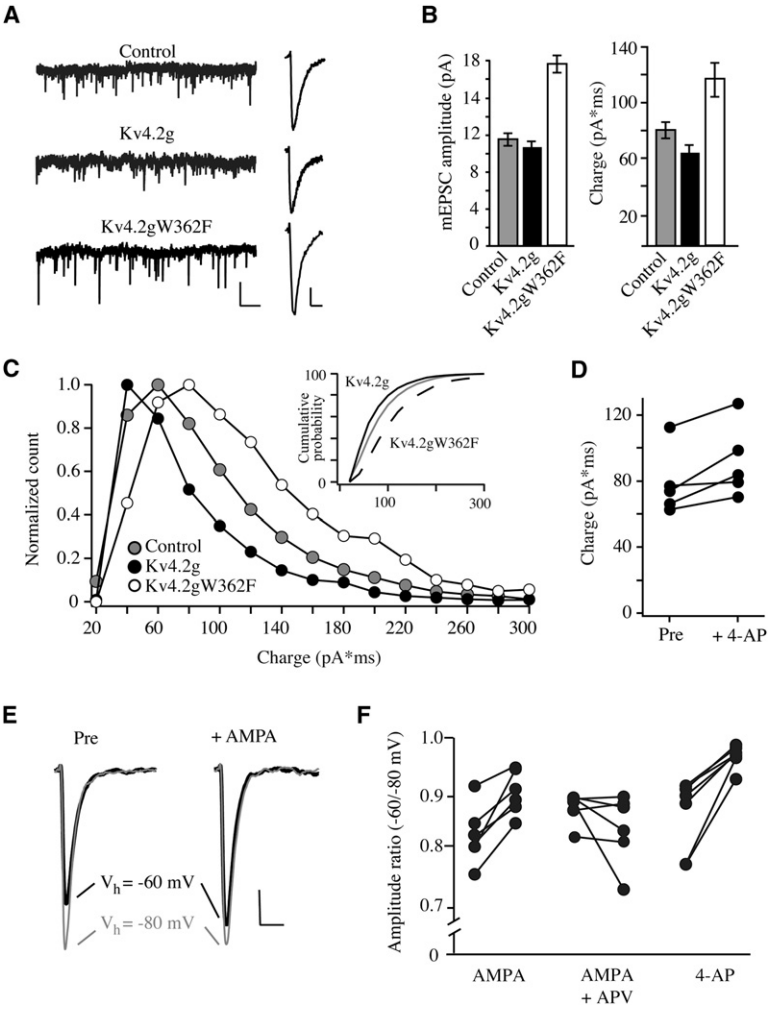

Figure 6. Kv4.2 Shapes mEPSCs

(A) Sample mEPSC recordings from control and Kv4.2g- and Kv4.2g^{W362F} -expressing neurons (left). Scale bar, 10 pA, 1 s. Aligned and averaged mEPSCs from the same cells as the traces to the left (right). Scale bar, 2.5 pA, 10 ms. (B) Pooled amplitude and charge data of mEPSCs from each experimental group. Both amplitude and charge are reduced in Kv4.2g-expressing neurons (black bar) and enhanced in Kv4.2g^{W362F} neurons (white bar) compared with control (gray bar). Error bars represent SEM. (C) Normalized count of mEPSC charge for each experimental group. Charges for the first 200 mEPSCs recorded for each cell were used to create the distributions. With increasing functional level of Kv4.2, the charge profile broadened and the peak shifted toward larger charges. The inset shows the cumulative probability of charge (binned into 20 pA*ms bins) for Kv4.2g-expressing neurons (black trace) and enhanced in Kv4.2g^{W362F} neurons (dashed trace) compared with control (gray trace). (D) Bath application of 4-AP (7 mM) significantly increased mEPSC charge in three of five cells tested. All recordings in (A)–(D) were made from a −60 mV holding potential. (E) AMPA stimulation reduces the A-type K^+ current effect on mEPSCs. Example mEPSCs measured from holding potentials around rest (−60 mV) and outside of the Kv4.2 activation range (−80 mV) before and after AMPA (25 μM, 2–3 min) stimulation. Each trace is the average of mEPSCs recorded for 5 min at each potential and condition. Scale bar, 5 pA, 5 ms. (F) In all six cells tested, AMPA stimulation increased the −60/−80 mV mEPSC amplitude ratio. This effect is consistent with Kv4.2 internalization, as it is blocked by coapplication of APV (50 μM) and mimicked by 4-AP (7 mM). Amplitude ratios in all conditions may be overestimates if we are measuring mEPSCs from a population of distal synapses in the −80 mV condition that, at −60 mV, do not rise above noise to a detectable level. These distal synapses have smaller amplitudes due to cable properties of the dendrite, thus reducing the average amplitude in the −80 recordings and increasing the ratio.

after bath-applied AMPA (25–50 μM, 2–3 min). Since this treatment causes not only Kv4.2 internalization but also AMPAR internalization (Figure 5) (Lin et al., 2000; Lissin et al., 1999), we report the ratio of mEPSCs recorded at −60 mV to those recorded at −80 mV. The rationale for this analysis is that, whereas AMPA-mediated EPSCs show a linear I-V relationship between rest and hyperpolarized potentials, a holding potential of −80 mV brings Kv4.2 channels out of their activation range (Kim et al., 2005). AMPA stimulation increased the −60/−80 mV mEPSC amplitude ratio in six of six cells (0.81 ± 0.02 to 0.91 ± 0.02, $p < 0.05$, Wilcoxon; Figures 6E and 6F). As with Kv4.2g internalization (Figure 3), this effect was blocked by preapplication of APV (0.87 ± 0.01 to 0.83 ± 0.03, $p > 0.05$, Wilcoxon; Figure 6F). Blocking A-type K^+ channels with 4-AP (7 mM) also increased the ratio (pre-4-AP, 0.86 ± 0.03 versus post-4-AP, 0.97 ± 0.01, $p < 0.05$, Wilcoxon; Figure 6F), showing that K^+ channels shape mEPSCs recorded at −60 mV.

Internalization of Kv4.2 Contributes to LTP

Our results demonstrate that activity-dependent internalization of Kv4.2 in active spines enhances their efficacy through an NMDAR- and Ca^{2+}-dependent mechanism. Because LTP shares these NMDAR and Ca^{2+} requirements for induction, we wondered if LTP induction would stimulate Kv4.2 internalization. A brief application of the NMDAR coagonist glycine has been shown previously to increase the amplitude and the frequency of spontaneous mEPSCs through synaptic GluR1 insertion (chem-LTP) (Lu et al., 2001). We too found enhanced mEPSC amplitude (120.6% ± 8.3% after 30 min; Figure S4) and surface GluR1 enhancement after chem-LTP in both control and

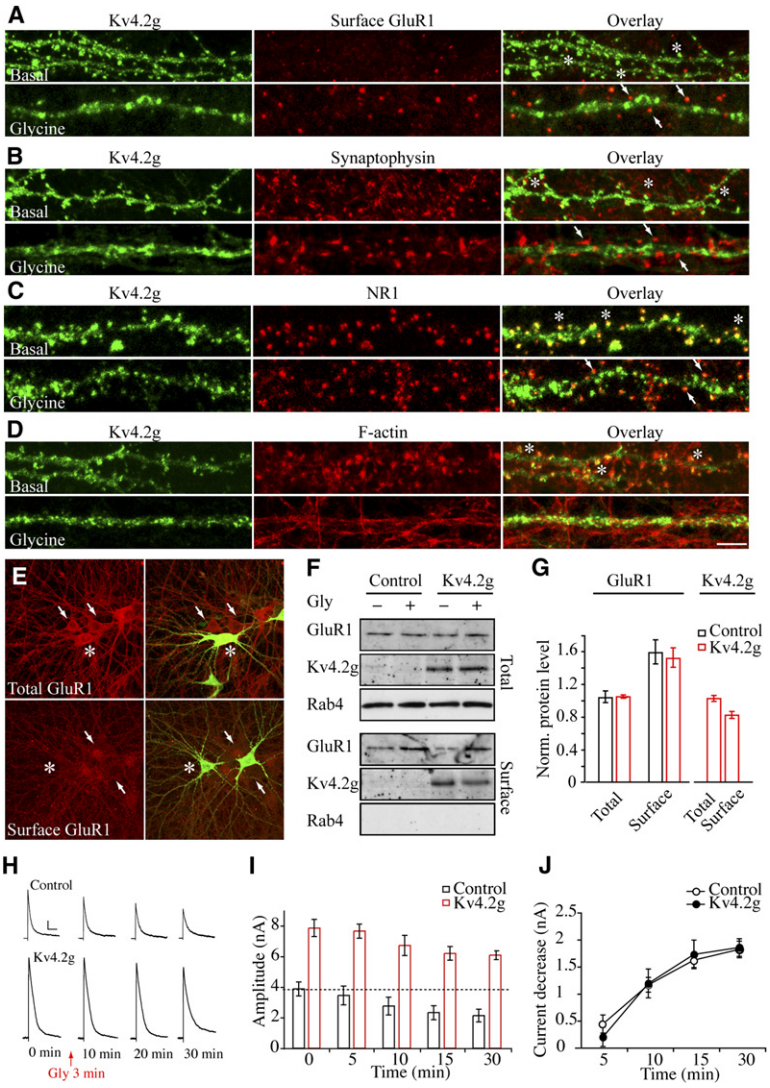

Figure 7. Chem-LTP Induces Synaptic Insertion of GluR1 but Also Kv4.2g Internalization

(A–D) Glycine (200 μM, 3–5 min) induced LTP enhanced surface expression of GluR1 while reducing the number of Kv4.2g puncta colabeled with synaptic markers. Asterisks, Kv4.2g-positive clusters; arrows, Kv4.2g-negative clusters. Scale bar, 8 μm.

(E) No significant differences in intensity of immunostained GluR1 were observed between Kv4.2g-expressing and control neurons. Levels of endogenous total and surface GluR1 were compared in Kv4.2g-expressing (asterisk) and control neurons (arrow).

(F) Total and surface levels of Kv4.2g and GluR1 were examined before and after LTP induction in Kv4.2g neurons using biotinylation and immunoblots.

(G) With chem-LTP (200 μM glycine, 3–5 min), surface Kv4.2g was reduced (~82%) and surface GluR1 was enhanced (~155%). Total protein levels of Kv4.2g and GluR1 were normalized to the control protein Rab4. Surface levels of two proteins were normalized to the corresponding total protein level. Normalized total and surface protein levels were then compared before and after chem-LTP induction. The enhanced level of surface GluR1 was similar in Kv4.2g and control neurons. Rab4 is shown as a cytoplasmic control. Error bars represent SEM.

(H) Examples of the decrease in transient K^+ currents during chem-LTP. A-type K^+ currents are decreased by Kv4.2 internalization during chem-LTP. Transient currents of each group were recorded from the same cell at the times indicated. Each trace is an average of five sweeps. Scale bar, 1 nA, 100 ms.

(I) Decrease in average transient K^+ current amplitude during chem-LTP. Transient K^+ currents were gradually and significantly decreased after chem-LTP induction in both groups. However, the remaining amplitude in Kv4.2g neurons was still greater than the basal level in control neurons, indicated by a dashed line.

(J) Cumulative decrease of transient K^+ currents during chem-LTP shows identical time courses and magnitudes for both groups. Error bars represent SEM.

Kv4.2g-expressing neurons (200 μM glycine, 3–5 min; Figures 7A and 7F).

However, chem-LTP induction also drove Kv4.2g *out* of spines (Figures 7A–7D). Similar to AMPA-stimulated internalization of Kv4.2g, the number of Kv4.2g puncta colabeled with Synaptophysin or NR1 was markedly decreased (Figures 7B and 7C). No significant change in NMDAR distribution after glycine treatment was detected by immunostaining (number of NR1 clusters per 10 μm dendrite: 6.76 ± 0.46, n = 17, pre-chem-LTP versus 6.80 ± 0.22, n = 21, post-chem-LTP). Chem-LTP also led to the reorganization of F-actin away from spines, forming tether-like filamentous structures in the dendritic shaft. Such reorganization was previously shown to be NMDAR dependent (Hering and Sheng, 2003). It is also important to note that no significant differences in expression level of total or surface AMPARs were observed between Kv4.2g-expressing and control neurons by immunostaining and blotting (Figures 7E–7G). A biotinylation assay confirmed that surface GluR1 increased similarly between the two groups (151.6% ± 11.8%, n = 3 for Kv4.2g-expressing versus 158.6% ± 14.7%, n = 4 for control) and that ~18% of Kv4.2g was internalized during chem-LTP (82.1% ± 4.2% of basal, n = 3; Figure 7G).

Consistent with these imaging results showing Kv4.2g internalization during chem-LTP, endogenous transient

K^+ current amplitude decreased in whole-cell recordings (60.0% ± 5.8%, n = 6, $p < 0.05$, paired Student's t test), with no significant change in sustained K^+ current amplitudes (96.5% ± 6.5%, n = 6, $p > 0.05$, paired Student's t test; Figures 7H and 7I). The time course of this current decrease is also similar to the time course of Kv4.2g internalization after AMPA stimulation measured in our live imaging experiments (Figures 3 and 7I and Movie S1). In addition, the chem-LTP-induced decrease in endogenous transient K^+ current was blocked by APV (*transient*, 100.9% ± 2.6%; *sustained*, 99.7% ± 3.3%, n = 5; data not shown). Notably, although a larger fraction of A-type K^+ channel density remains in Kv4.2g-expressing neurons after chem-LTP stimulation compared to control (Figures 7H and 7I), the absolute magnitude of decrease in peak transient K^+ current density is constant in both Kv4.2g-expressing and control neurons (1.78 ± 0.09 nA for Kv4.2g-expressing versus 1.74 ± 0.12 nA for control; Figure 7J). This fixed capacity for Kv4.2 internalization in response to synaptic activity could be due to limitations of the endogenous Kv4.2-related endocytosis machinery. Taken together, these results show that the cellular mechanism of chem-LTP expression is associated with a specific decrease in functional A-type K^+ channels, along with the increase in synaptic AMPARs.

We also found evidence for Kv4.2 internalization after synaptically evoked LTP induction in hippocampal organotypic slice cultures (Figure 8). Here, we measured evoked synaptic currents alternatively at −60 and −80 mV. The −60/−80 mV ratio was monitored before and after LTP induced by a pairing protocol (Barria and Malinow, 2005). Figure 8A shows an individual experiment where we plot the percent change in EPSC amplitude at the two holding potentials after LTP. The amount of potentiation observed was greater at −60 mV than at −80 mV, resulting in an increase in −60/−80 mV ratio. Enhanced potentiation at −60 mV compared to −80 mV was observed in seven of seven neurons tested (average EPSC change 30–35 min post-LTP: $V_{H\text{-}60\ mV}$ = 88% ± 15%, $V_{H\text{-}80\ mV}$ = 51% ± 16%, $p < 0.05$, Wilcoxon; Figure 8B). The average −60/−80 mV EPSC ratio increased from 0.57 ± 0.04 pre-LTP induction to 0.79 ± 0.07 30 min post-LTP induction. Only synapses receiving stimulation during pairing displayed any potentiation at either holding potential, showing that Kv4.2 internalization is specific to potentiated synapses (Figure 8B, "unpaired"). These results are consistent with synapse-specific Kv4.2 internalization as a contributing factor to LTP.

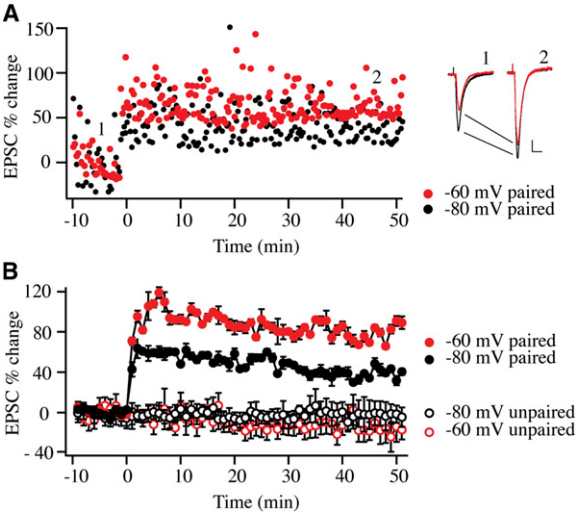

Figure 8. Evidence for Kv4.2 Internalization during Synaptically Evoked LTP

(A) An example of LTP induced in a CA1 pyramidal neuron from an organotypic slice. EPSCs were measured alternatively at −60 (red circles) and −80 mV (black circles) every 20 s. LTP was induced using a depolarization pairing protocol. LTP was greater in the −60 mV traces than in those recorded from a holding potential of −80 mV. Inset shows EPSCs for each holding potential before (1) and 45 min after (2) LTP induction. As after AMPA stimulation in mEPSC recordings (Figure 6), LTP reduced the −60/−80 mV EPSC ratio, consistent with Kv4.2 internalization. Each trace is an average of three EPSCs. Scale bar, 25 pA, 25 ms.

(B) Pooled LTP data from seven cells. After confirming LTP in each neuron, we compared the degree of potentiation at the −60 mV holding potential to that recorded at −80 mV over the final 5 min of recordings. Potentiation was greater for the −60 mV holding potential in every cell tested. No potentiation was observed at either holding potential in six cells where EPSCs from a second, control pathway (not receiving synaptic stimulation during the depolarization used to induce LTP) were evoked with a second stimulating electrode. Error bars represent SEM.

DISCUSSION

Our primary finding is the activity-dependent redistribution of the dendritic voltage-gated K^+ channel subunit, Kv4.2, out of spines of cultured hippocampal neurons. This internalization enhanced mEPSC efficacy and shares common requirements for induction with LTP, namely, NMDAR activation and Ca^{2+} influx. Whole-cell voltage-clamp recordings demonstrated that stimulations inducing Kv4.2 internalization result in a specific reduction of endogenous A-type K^+ currents upon synaptic activation. LTP induced by brief glycine application resulted in synaptic GluR1 insertion but also Kv4.2 internalization. In addition, we provide evidence for Kv4.2 internalization as a contributing factor to synaptically evoked LTP. These results present a mechanism for controlling synaptic integration through regulation of the surface expression level of voltage-gated A-type K^+ channels.

Physiological Relevance of Kv4.2g Internalization

Although the large number of synapses stimulated in our imaging experiments resulted in Kv4.2g internalization in both spines and the dendritic shaft, computer modeling suggests that the major effect of A-type channels on synaptic events occurs at the site of input and that the relative amount of voltage attenuation from dendrite to soma is unchanged by 4-AP application (Hoffman et al., 1997). Our previous results showing enriched spine expression of Kv4.2g (Kim et al., 2005), along with the present

demonstration of activity-dependent removal of Kv4.2g from spines (Figure 1 and Figure S2), suggest a specific role of spine Kv4.2 in regulating synaptic activity during normal synaptic input. Such an arrangement may facilitate the synapse specificity of internalization and its effect on synaptic efficacy. Previously it was shown that A-type K^+ channels act to prevent subthreshold Na^+ channel activation, countering Na^+ channel EPSP boosting (Hoffman et al., 1997). Kv4.2 internalization would thus be expected to enhance synaptic potentials by removing this block to Na^+ channel activation.

It is important to question whether our results showing Kv4.2g internalization occur normally for endogenous Kv4.2. A number of observations provide strong evidence that the activity-dependent regulation of the Kv4.2 represents a physiological mechanism for controlling excitability. (1) In Figure 1, we show that both Kv4.2g and endogenous Kv4.2 membrane fractions are reduced upon AMPA stimulation in biotinylation experiments. (2) Kv4.2g expression did not alter the expression levels or trafficking behavior of endogenous GluR1 and NMDARs. (3) We found no differences in synaptic structure or number in Kv4.2g-expressing neurons compared with control. (4) We show here that both Kv4.2g and endogenous Kv4.2 are located in hippocampal spines. (5) AMPA stimulation and chem-LTP induction both result in a specific decrease in *endogenous* transient (but not sustained) K^+ currents as well as Kv4.2g internalization (assessed by fluorescent imaging and biotinylation assays). (6) Both activity-dependent Kv4.2g internalization and endogenous A-type K^+ current decreases are blocked by APV. (7) Both AMPA-induced Kv4.2g internalization and endogenous A-type K^+ current decreases are blocked by an active dynamin peptide. (8) Blocking endocytosis with the dynamin peptide reduced AMPA-induced depolarization. (9) In chem-LTP experiments, control and Kv4.2g-expressing neurons displayed nearly identical reductions (magnitude and time course) in transient K^+ current amplitudes. And finally, (10) LTP was reduced by hyperpolarization, consistent with Kv4.2 internalization during synaptically evoked LTP.

Role of Kv4.2 in Synaptic Plasticity

Accumulating evidence shows that synaptic plasticity is at least partially accomplished through the trafficking of postsynaptic receptor proteins in hippocampal neurons (Barry and Ziff, 2002; Collingridge et al., 2004). In particular, the insertion or removal of synaptic AMPARs is thought to determine the direction of synaptic plasticity (potentiation or depression) (Brown et al., 2005; Malinow and Malenka, 2002; Man et al., 2000; Shi et al., 1999). Here, we provide evidence that the regulated surface expression of a dendritic voltage-gated transient K^+ channel serves as an additional contributor to synaptic plasticity. In support of previous reports showing that A-type K^+ currents regulate EPSP amplitude in hippocampal neurons, we found that decreasing functional Kv4.2 expression levels enhanced the average amplitude and charge of mEPSCs recorded in the soma (Hoffman et al., 1997; Ramakers and Storm, 2002). Given the distinctive responses of Kv4.2 and GluR1, we can now say that postsynaptic protein trafficking during chem-LTP is, in effect, a two-way street. This finding raises the question of how neurons distinguish and control movement of different types of channels. Whether surface expression of other dendritic voltage-gated ion channels is also regulated by synaptic activity and knowledge of the conditions under which channels are reinserted back into the membrane calls for further study. Future studies will also elucidate the molecular pathways and mechanisms of activity-dependent Kv4.2 internalization and reinsertion, including the potential role of posttranslational modifications and binding partners.

Excitatory neuronal stimulation with either AMPA application or chem-LTP induction caused Kv4.2 internalization. In contrast, GluR1 has opposing responses to the two stimulations with AMPA stimulation causing internalization (Figure 5) but chem-LTP enhancing surface expression (Figure 7). Some resolution for this disparate molecular behavior comes from the observation that GluR1 internalization by ligand binding (AMPA stimulation) is mimicked by CNQX and does not require NMDAR activation and thus is not a specific response to activity (Lin et al., 2000).

A previous report has found that LTP induction in acute hippocampal slices results in a hyperpolarizing shift in dendritic transient K^+ current inactivation curve, enhancing backpropagating action potential amplitude (Frick et al., 2004). While numerous methodological differences prevent a direct comparison between the two studies, our results are not necessarily mutually exclusive. Although Frick et al. did not report a specific decrease in peak transient K^+ channel amplitude with LTP in cell-attached dendritic patches, their LTP induction may indeed cause internalization, which is not detected in the cell-attached patch because the machinery is compromised during patch formation and/or because the patch is physically too distant from the potentiated synapses. On the other hand, the inactivation curve shift seen in dendritic patches by Frick et al. may also occur with chem-LTP. This curve shift would not be expected to contribute to the decrease in transient K^+ currents we observed (Figure 7), given that their measurement followed a hyperpolarizing prepulse to -120 mV, removing inactivation even with the inactivation curve shift. In our pairing-induced LTP in CA1 neurons from hippocampal organotypic slices, outside-out patches pulled 30 min after LTP induction revealed transient K^+ current inactivation curves identical to control (S.-C. J., unpublished data). Thus, our reported difference between potentiation measured at -60 and -80 mV (Figure 8) cannot be explained by a K^+ current inactivation curve shift at this time point. More recently, the same group has shown enhanced induction of long-term potentiation in hippocampal CA1 pyramidal neurons of Kv4.2 knockout mice, suggesting a potential role for Kv4.2 trafficking in metaplasticity (Abraham and Bear, 1996; Chen et al., 2006).

Kv4.2 Trafficking and Dendritic Excitability

Transient K^+ channels regulate a number of other measures of excitability, including the backpropagation of action potentials in dendrites of hippocampal neurons, action potential initiation in dendrites, the propagation of dendritic Ca^{2+} plateau potentials, action potential half-width, and frequency-dependent action potential broadening (Cai et al., 2004; Frick et al., 2004; Hoffman et al., 1997; Kim et al., 2005; Losonczy and Magee, 2006). Recent evidence shows that Kv4.2 prevents plateau potentials from propagating past branch points (Cai et al., 2004), that transient K^+ currents shaped fast Na^+ spikes in oblique CA1 pyramidal neuron dendrites (Losonczy and Magee, 2006), and that Kv4.2 is clustered at GABAergic as well as glutamatergic synapses (Burkhalter et al., 2006; Jinno et al., 2005; Kollo et al., 2006). Kv4.2 endocytosis may then have different effects on integration for different populations of Kv4.2-containing channels depending on their location in the dendrite. Likewise, targeted insertion of Kv4.2 into specific dendritic compartments may be employed by neurons to shape dendritic integration and backpropagation.

Here we have shown that Kv4.2 internalization occurs after global synaptic activation with AMPA, mimicking a large, distributed barrage of synaptic activity. This activity would also be expected to affect suprathreshold dendritic signals controlled by Kv4.2, such as dendritic action potential backpropagation, furthering dendritic Ca^{2+} influx and excitability. Such highly synchronized and frequent discharges occur during epileptic seizures. Recently, a Kv4.2 truncation mutation was found in a patient with temporal lobe epilepsy (Singh et al., 2006), and studies in epilepsy models have demonstrated an activity-dependent downregulation of Kv4.2 channels (Bernard et al., 2004; Tsaur et al., 1992). Kv4.2 internalization may then be a contributing factor to the hyperexcitability observed in temporal lobe epilepsy and/or may play an important role in susceptibility to seizure onset in the hippocampus.

EXPERIMENTAL PROCEDURES

Hippocampal Cultures and Viral Infection

Hippocampal primary cultures were prepared from embryonic day 18 Sprague-Dawley rats as per Osten et al. (1998) with the exception of coverslip coating. Here, hippocampi were triturated 15 min after trypsinization and plated on coverslips coated with poly-D-lysine (50 μg/ml, Sigma) and laminin (5 μg/ml, Invitrogen). Dissociated neurons were cultured in neurobasal medium supplemented with B27 (Invitrogen). To eliminate proliferative glia cells, 5 μM cytosine arabinoside (AraC, Sigma), a specific inhibitor of DNA synthesis during meiosis and mitosis, was included after 8 DIV. Primary neurons were infected with a normalized infectious titer of modified Sindbis virus resulting in 10%–20% infection of neurons for imaging and electrophysiological experiments 1 day before use and ~30% for biotinylation. Attenuated Sindbis viruses expressing EGFP-tagged Kv4.2 and EGFP alone were produced using the SINrep(nsP2S^{726}) viral vector and DH-BB(tRNA/TE12) helper plasmid as described (Kim et al., 2004). The improved red fluorescent protein (tdTomato, provided by Dr. Tsien [Shaner et al., 2004]), a tandem dimer variant of DsRed, was transfected by Nucleofection (Amaxa Biosystems) in accordance with the manufacturer's protocol. Other constructs used in present experiments were described previously (Kim et al., 2005). Hippocampal organotypic slice cultures (400 μm thick) were prepared from postnatal day 7–8 Sprague-Dawley rats after Shi et al. (1999). Hippocampal CA1 neurons were infected on 4 DIV by microinjection (Nanoliter 2000, World Precision Instruments). All animal procedures were conducted with accordance of the National Institutes of Health Guide for the Care and Use of Laboratory Animals under a protocol approved by the National Institutes of Child Health and Human Development's Animal Care and Use Committee.

Biotinylation Assay and Immunoblots

Hippocampal neurons (18–24 DIV) or acute slices (postnatal day 14) were incubated with freshly made sulfosuccinimidyl-2-(biotinamido) ethyl-1,3-dithiopropionate (sulfo-NHS-SS-biotin, 1 mg/ml, Pierce) in ice-cold PBS for 30 min at 4°C, followed by 10 min incubation in ice-cold glycine (100 mM) at 4°C, and lysed with lysis buffer containing 25 mM HEPES (pH 7.4), 150 mM NaCl, 1% Triton X-100, 0.05% SDS, and a protease inhibitor mixture tablet (Roche). The lysate was incubated at 4°C for 20 min and spun at 13,000 rpm for 10 min. Biotin-labeled surface proteins were precipitated with 20–30 μl of immobilized Streptavidin beaded agarose (Pierce) at 4°C overnight. The beads were washed five times with lysis buffer, and proteins were eluted in 2× SDS loading buffer. Immunoblotting was performed as described (Kim et al., 2005). Antibodies were as follows: anti-GFP (Molecular Probes, 1:5000), anti-GluR1-C (Chemicon, 1:200), anti-Kv4.2 (K57/1, NeuroMab, 1:1000), and anti-Rab4 (BD Transduction Laboratories, 1:1000).

Fluorescence Staining

Treatments

Hippocampal neurons (18–24 DIV) were stimulated for imaging and biotinylation assays in culture media with either KCl (50 mM, Sigma), glutamate (50 μM, Sigma), NMDA (20 μM, Tocris), or (S)-AMPA (100 μM, Tocris) at 37°C for 15 min. Due to activity-dependent filamentous structural change of F-actin in these experiments (Halpain et al., 1998; Hering and Sheng, 2003), a more mild stimulation was achieved by reducing the concentration of stimulants (25 mM KCl, 50 μM AMPA). All blockers were applied 15 min prior to stimulation. The blockers used in the experiments were 100 μM D,L-APV, 50 μM CNQX, 1 μM TTX, 20 nM TeTN (Sigma), and 10 μM BAPTA-AM (Molecular Probes). Myristoylated DYN peptide (myrs-QVPSRPNRAP) and scrambled DYN (myrs-QPPASNPRVR) were synthesized and purified by Sigma Genosys. Peptides (50 μM) were applied 10 min prior to AMPA stimulation. For the chemical LTP induction, 200 μM glycine was bath applied in the Mg-free ACSF containing the following: 125 mM NaCl, 25 mM $NaHCO_3$, 2.5 mM KCl, 1.25 mM NaH_2PO_4, 2 mM $CaCl_2$, 11 mM D-glucose, 0.0005 mM TTX, 0.001 mM strychnine, and 0.02 mM bicuculine (pH 7.2) at 37°C for 3–5 min. Neurons were then incubated in the same ACSF without glycine at 37°C for 20 min. Treated neurons were always compared to simultaneously prepared sister culture controls.

F-Actin Staining

Treated neurons were immediately fixed with 4% paraformaldehyde and 0.1% glutaraldehyde in PBS containing 0.12 M sucrose for 8 min on ice and permeabilized with 0.5% Triton X-100 in PBS for 5 min. Actin was labeled with tetramethylrhodamine isothiocyanate (TRITC)-conjugated phalloidin (0.5 μM, Sigma) in PBS containing 1% BSA for 5 min.

Immunostaining

Neurons were fixed/permeabilized as described above for GluR1 and Synaptophysin staining or fixed with −20°C methanol for NMDAR1. After preblocking with PBS containing 5% NGS, 0.05% Triton X-100, and 450 mM NaCl for 1 hr at 4°C, neurons were incubated with antibodies in the blocking solution overnight at 4°C and followed by incubation with Alexa 546-conjugated secondary antibodies (Molecular Probes) for 2 hr at RT. To label surface AMPARs, nonpermeabilized neurons

were incubated with anti-GluR1-N in PBS containing 1% BSA and 4% NGS at 4°C overnight. Antibodies were as follows: Alexa 488-labeled anti-GFP (Molecular Probes, 1:10,000), anti-GluR1-N (Calbiochem, 1:20), anti-GluR1-C (Chemicon, 1:200), anti-NMDAR1 (Chemicon, 1:100), and anti-Synaptophysin (Sigma, 1:200).

Image Acquisition and Analysis

Fixed cell images were acquired with a Leica TCS RS confocal microscope. The same instrument parameter settings were kept for each experiment. Every experiment was repeated a minimum of five times. The two fluorophores were excited with different wavelengths, 488 and 543 nm, and were separately imaged using dual sequential scanning to avoid overlapped emission from one to the other. Acquired images were analyzed using MetaMorph v6.3 (Universal Imaging Corporation) and ImageJ v1.36 (http://rsb.info.nih.gov/ij/) under the same analytic parameter settings for each channel. To determine the number of Kv4.2g-positive spines or colabeled clusters, marker-labeled spines or puncta (clusters) were randomly selected on 6 to 27 neurons (260 to 1400 spines) using a 1.7 μm diameter circle region of interest (ROI). Pixels above the threshold intensity were counted and logged into Excel (Microsoft). To compare the colocalization of Kv4.2g and GluR1, fluorescent intensity was line plotted by manually drawing a line either inside or outside of dendrites (range 0–255, arbitrary units).

Live imaging was performed at the NICHD Microscopy & Imaging Core using a Zeiss LSM 510 Inverted Meta with 100× Zeiss α plan-neofluar oil objective (http://mic.nichd.nih.gov/index.htm). Hippocampal primary neurons transfected with the tdTomato were plated on 25 mm coverslips and then infected with modified Sindbis virus expressing Kv4.2g on 18–24 DIV. Coverslips containing Kv4.2g- and tdTomato-coexpressed neurons were placed in an Attofluor cell chamber (Molecular Probes) and perfused with Mg-free ACSF containing the following: 125 mM NaCl, 25 mM $NaHCO_3$, 2.5 mM KCl, 1.25 mM NaH_2PO_4, 2 mM $CaCl_2$, 11 mM D-glucose (pH 7.2). The neurons, objective, and stage were heated in a custom-built incubation chamber supplemented with 5% CO_2. Time-lapse images were captured every 1 min for 15–20 min at 37°C using Zeiss LSM Image Browser software v3.2. The instrument parameter settings were optimized in unstimulated Kv4.2g-expressing neurons to avoid photobleaching and image saturation. Each image was a maximal projection of five to seven z stacks obtained at 0.5 μm depth intervals. Projection images generated for each time points were analyzed using MetaMorph, ImageJ, and Zeiss software. Spines were identified by tdTomato signal and randomly selected using ROIs. All spines identified in the first time point were followed for all the sequent time images, and thus selection was blind regarding the consequence. For dendritic shaft analysis, the ROI was moved to the shaft directly below the spine. Fluorescent signals of Kv4.2g within the ROI were then measured. Fluorescent changes (ΔF) in Kv4.2g intensity were calculated after normalizing by the tdTomato intensity value in each time point using the initial green fluorescence (F_0) prior to stimulation as a baseline. Hence, fractional fluorescent change in each time trace was represented by $\Delta F/F_0$ = (normalized F − normalized F_0)/normalized F_0. The data were averaged from 75 to 195 spines of four to nine neurons from at least six independent experiments. Averaged values were presented as means ± standard error of the mean (SEM).

Electrophysiology

Thick-walled, filamented patch electrodes had tip resistances of 3–6 MΩ. Series resistance varied between 8–30 MΩ, and recordings where series resistance varied by more than 10% were rejected. No electronic compensation for series resistance was employed. All electrophysiological data were recorded using an Axopatch200B amplifier (Molecular Devices Corp.). Recordings were filtered at 2 kHz for mEPSCs and at 5 kHz for K^+ currents and evoked EPSCs. Command pulse generation, data acquisition, and analysis were performed using IGOR Pro (Wavemetrics). MiniAnalysis (Synaptosoft), SPSS (SPSS Inc.), and Excel (Microsoft) software were used for further data and statistical analysis. One-way ANOVA, Wilcoxon signed rank, and Student's t tests were used to examine statistical significance, set to $p < 0.05$.

K^+ Current Recordings

Transient K^+ currents were measured in young hippocampal primary neurons (7–8 DIV). These smaller neurons, possessing fewer dendritic processes, were used to limit space-clamp and access resistance errors associated with whole-cell recordings of large (nA) currents. Electrodes were filled with a solution containing the following: 140 mM KCl, 2 mM $MgCl_2$, 10 mM HEPES, 5 mM EGTA, 5 mM ATP, 1 mM $CaCl_2$, 10 mM D-glucose (pH 7.3 with KOH). TTX (1 μM) was added to the external solution to block voltage-gated Na^+ currents except during AMPA stimulation. After recording K^+ currents, AMPA (50 μM, 5 min) or glycine (200 μM, 3 min) containing external solution was applied and currents were recorded every 5 min for 30 min. Transient and sustained K^+ currents were digitally separated using a prepulse protocol after the subtraction of leak currents. Peak currents were measured at +120 mV after a 400 ms prepulse to either −120 mV or +30 mV. Nonmyristoylated DYN peptide (QVPSRPNRAP, 100 μg/ml) or scrambled DYN (QPPASNPRVR, 100 μg/ml) was coapplied in internal solution, 20–25 min prior to AMPA stimulation. During and after AMPA stimulation, resting membrane potential was monitored. Cells depolarizing beyond −30 mV during AMPA stimulation were not analyzed. Glycine application depolarized cells up to −45 mV. Cells that did not recover to −60 mV after 5 min of AMPA or glycine washout were also not analyzed.

mEPSC Recordings

For recording mEPSCs, primary dissociated culture neurons of 14–21 DIV were used. The patch electrode solution contained either the same internal solution listed above for K^+ current recordings (mEPSC amplitude ratio experiments, in some cases without $MgCl_2$) or, for chem-LTP experiments, the following: 100 mM Cs-gluconate, 5 mM $MgCl_2$, 0.6 mM EGTA, 8 mM NaCl, 40 mM HEPES, 2 mM NaATP, 0.3 mM TrisGTP (pH 7.2 with KOH). TTX (0.5–1 μM), strychnine (1 μM), and bicuculine (20 μM) were included in the external solution during all mEPSC recordings. After whole-cell formation, a 5–10 min recovery period elapsed before data collection. Ten seconds of spontaneous activity were recorded every 30 s for each holding potential. mEPSC data were then averaged over a 5 min period (total sampling duration of 100 s/5 min period) for up to 60 min. Only 5 min periods exhibiting more than ten events and average decay times of less than 10 ms were analyzed. Neurons not recovering to within 10 mV of their resting membrane potential within 20 min after AMPA stimulation (25 μM, 2–3 min) were not analyzed. For amplitude and ratio experiments, two to three episodes (10–15 min of data) were averaged before and after each condition. For chem-LTP analysis, the largest 20% of mEPSC amplitudes for each 5 min period were averaged to reduce the impact of nonspecific frequency changes (Stell and Mody, 2002).

Hippocampal Organotypic Slice Culture Recordings

Hippocampal organotypic slice cultures were transferred to a submerged recording chamber with a continuous flow of ACSF containing the following: 125 mM NaCl, 2.5 mM KCl, 25 mM NaHCO3, 1.25 mM NaH_2PO_4, 25 mM glucose, 2 mM $CaCl_2$, 1 mM $MgCl_2$, 0.005 mM bicuculine (pH 7.4) and bubbled with 5% CO_2/95% O_2. In all experiments, 5 μM 2-chloroadenosine was included in the external solution to block recurrent synaptic connections. The patch electrodes were filled with the following: 20 mM KCl, 125 mM Kglu, 10 mM HEPES, 4 mM NaCl, 0.5 mM EGTA, 4 mM APT, 0.3 mM TrisGTP, 10 mM Phosphocreatin (pH 7.2). To record EPSCs at several holding potentials, whole-cell CA1 pyramidal neuron recordings were made in voltage-clamp mode at 31°C–32°C. The pathway between CA1 and CA3 was cut before each experiment. EPSCs were elicited by a test pulse (0.2 ms duration at 0.1 Hz, 30–600 μA amplitude), alternatively at −60 or −80 mV through a glass bipolar electrode (10 μm tip) located at the Schaffer collateral pathway. For LTP induction, 2 Hz stimulation was paired

with depolarization to 0 mV for 1 min. In some experiments a second stimulating electrode was used to record EPSCs in a control (unpaired) pathway. Pathway independence was measured using a cross-paired-pulse facilitation protocol. LTP-induced changes of EPSC amplitude were monitored for up to 1 hr (but at least 40 min).

Supplemental Data

The Supplemental Data for this article can be found online at http://www.neuron.org/cgi/content/full/54/6/933/DC1/.

ACKNOWLEDGMENTS

We thank Drs. Rebecca Hammond, Pavel Osten, and Chris McBain for their critical review of versions of this manuscript; Arrash Yazdani for technical support; and Dr. Ya-Xian Wang for help with the immunogold study. Live imaging was performed at the NICHD Microscopy & Imaging Core with the assistance of Dr. Vincent Schram and Chip Dye. This work was supported by the National Institute of Child Health and Human Development Intramural Research Program.

Received: February 17, 2006
Revised: September 6, 2006
Accepted: May 23, 2007
Published: June 20, 2007

REFERENCES

Abraham, W.C., and Bear, M.F. (1996). Metaplasticity: The plasticity of synaptic plasticity. Trends Neurosci. *19*, 126–130.

Alonso, G., and Widmer, H. (1997). Clustering of KV4.2 potassium channels in postsynaptic membrane of rat supraoptic neurons: An ultrastructural study. Neuroscience *77*, 617–621.

Barrett, J.N., and Crill, W.E. (1974). Influence of dendritic location and membrane properties on the effectiveness of synapses on cat motoneurones. J. Physiol. *239*, 325–345.

Barria, A., and Malinow, R. (2005). NMDA receptor subunit composition controls synaptic plasticity by regulating binding to CaMKII. Neuron *48*, 289–301.

Barry, M.F., and Ziff, E.B. (2002). Receptor trafficking and the plasticity of excitatory synapses. Curr. Opin. Neurobiol. *12*, 279–286.

Beattie, E.C., Carroll, R.C., Yu, X., Morishita, W., Yasuda, H., von Zastrow, M., and Malenka, R.C. (2000). Regulation of AMPA receptor endocytosis by a signaling mechanism shared with LTD. Nat. Neurosci. *3*, 1291–1300.

Bernard, C., Anderson, A., Becker, A., Poolos, N.P., Beck, H., and Johnston, D. (2004). Acquired dendritic channelopathy in temporal lobe epilepsy. Science *305*, 532–535.

Brebner, K., Wong, T.P., Liu, L., Liu, Y., Campsall, P., Gray, S., Phelps, L., Phillips, A.G., and Wang, Y.T. (2005). Nucleus accumbens long-term depression and the expression of behavioral sensitization. Science *310*, 1340–1343.

Bredt, D.S., and Nicoll, R.A. (2003). AMPA receptor trafficking at excitatory synapses. Neuron *40*, 361–379.

Brown, T.C., Tran, I.C., Backos, D.S., and Esteban, J.A. (2005). NMDA receptor-dependent activation of the small GTPase Rab5 drives the removal of synaptic AMPA receptors during hippocampal LTD. Neuron *45*, 81–94.

Burkhalter, A., Gonchar, Y., Mellor, R.L., and Nerbonne, J.M. (2006). Differential expression of I(A) channel subunits Kv4.2 and Kv4.3 in mouse visual cortical neurons and synapses. J. Neurosci. *26*, 12274–12282.

Cai, X., Liang, C.W., Muralidharan, S., Kao, J.P., Tang, C.M., and Thompson, S.M. (2004). Unique roles of SK and Kv4.2 potassium channels in dendritic integration. Neuron *44*, 351–364.

Carnevale, N.T., and Johnston, D. (1982). Electrophysiological characterization of remote chemical synapses. J. Neurophysiol. *47*, 606–621.

Carroll, R.C., Lissin, D.V., von Zastrow, M., Nicoll, R.A., and Malenka, R.C. (1999). Rapid redistribution of glutamate receptors contributes to long-term depression in hippocampal cultures. Nat. Neurosci. *2*, 454–460.

Cash, S., and Yuste, R. (1998). Input summation by cultured pyramidal neurons is linear and position-independent. J. Neurosci. *18*, 10–15.

Chen, X., Yuan, L.L., Zhao, C., Birnbaum, S.G., Frick, A., Jung, W.E., Schwarz, T.L., Sweatt, J.D., and Johnston, D. (2006). Deletion of Kv4.2 gene eliminates dendritic A-type K+ current and enhances induction of long-term potentiation in hippocampal CA1 pyramidal neurons. J. Neurosci. *26*, 12143–12151.

Collingridge, G.L., Isaac, J.T., and Wang, Y.T. (2004). Receptor trafficking and synaptic plasticity. Nat. Rev. Neurosci. *5*, 952–962.

Damke, H. (1996). Dynamin and receptor-mediated endocytosis. FEBS Lett. *389*, 48–51.

Ehlers, M.D. (2000). Reinsertion or degradation of AMPA receptors determined by activity-dependent endocytic sorting. Neuron *28*, 511–525.

Faber, E.S., Delaney, A.J., and Sah, P. (2005). SK channels regulate excitatory synaptic transmission and plasticity in the lateral amygdala. Nat. Neurosci. *8*, 635–641.

Frick, A., Magee, J., and Johnston, D. (2004). LTP is accompanied by an enhanced local excitability of pyramidal neuron dendrites. Nat. Neurosci. *7*, 126–135.

Groc, L., Heine, M., Cognet, L., Brickley, K., Stephenson, F.A., Lounis, B., and Choquet, D. (2004). Differential activity-dependent regulation of the lateral mobilities of AMPA and NMDA receptors. Nat. Neurosci. *7*, 695–696.

Halpain, S., Hipolito, A., and Saffer, L. (1998). Regulation of F-actin stability in dendritic spines by glutamate receptors and calcineurin. J. Neurosci. *18*, 9835–9844.

Hering, H., and Sheng, M. (2003). Activity-dependent redistribution and essential role of cortactin in dendritic spine morphogenesis. J. Neurosci. *23*, 11759–11769.

Hoffman, D.A., and Johnston, D. (1998). Downregulation of transient K+ channels in dendrites of hippocampal CA1 pyramidal neurons by activation of PKA and PKC. J. Neurosci. *18*, 3521–3528.

Hoffman, D.A., Magee, J.C., Colbert, C.M., and Johnston, D. (1997). K+ channel regulation of signal propagation in dendrites of hippocampal pyramidal neurons. Nature *387*, 869–875.

Jerng, H.H., Pfaffinger, P.J., and Covarrubias, M. (2004). Molecular physiology and modulation of somatodendritic A-type potassium channels. Mol. Cell. Neurosci. *27*, 343–369.

Jinno, S., Jeromin, A., and Kosaka, T. (2005). Postsynaptic and extrasynaptic localization of Kv4.2 channels in the mouse hippocampal region, with special reference to targeted clustering at gabaergic synapses. Neuroscience *134*, 483–494.

Kim, J., Dittgen, T., Nimmerjahn, A., Waters, J., Pawlak, V., Helmchen, F., Schlesinger, S., Seeburg, P.H., and Osten, P. (2004). Sindbis vector SINrep(nsP2S726): A tool for rapid heterologous expression with attenuated cytotoxicity in neurons. J. Neurosci. Methods *133*, 81–90.

Kim, J., Wei, D.S., and Hoffman, D.A. (2005). Kv4 potassium channel subunits control action potential repolarization and frequency-dependent broadening in rat hippocampal CA1 pyramidal neurones. J. Physiol. *569*, 41–57.

Kollo, M., Holderith, N.B., and Nusser, Z. (2006). Novel subcellular distribution pattern of A-type K+ channels on neuronal surface. J. Neurosci. *26*, 2684–2691.

Lin, J.W., Ju, W., Foster, K., Lee, S.H., Ahmadian, G., Wyszynski, M., Wang, Y.T., and Sheng, M. (2000). Distinct molecular mechanisms

and divergent endocytotic pathways of AMPA receptor internalization. Nat. Neurosci. *3*, 1282–1290.

Lipowsky, R., Gillessen, T., and Alzheimer, C. (1996). Dendritic Na+ channels amplify EPSPs in hippocampal CA1 pyramidal cells. J. Neurophysiol. *76*, 2181–2191.

Lissin, D.V., Carroll, R.C., Nicoll, R.A., Malenka, R.C., and von Zastrow, M. (1999). Rapid, activation-induced redistribution of ionotropic glutamate receptors in cultured hippocampal neurons. J. Neurosci. *19*, 1263–1272.

Losonczy, A., and Magee, J.C. (2006). Integrative properties of radial oblique dendrites in hippocampal CA1 pyramidal neurons. Neuron *50*, 291–307.

Lu, W., Man, H., Ju, W., Trimble, W.S., MacDonald, J.F., and Wang, Y.T. (2001). Activation of synaptic NMDA receptors induces membrane insertion of new AMPA receptors and LTP in cultured hippocampal neurons. Neuron *29*, 243–254.

Magee, J.C. (1999). Voltage-gated ion channels in dendrites. In Dendrites, G. Stuart, N. Spruston, and M. Hausser, eds. (Oxford: Oxford University Press), pp. 139–160.

Magee, J.C., and Johnston, D. (1995). Synaptic activation of voltage-gated channels in the dendrites of hippocampal pyramidal neurons. Science *268*, 301–304.

Malin, S.A., and Nerbonne, J.M. (2000). Elimination of the fast transient in superior cervical ganglion neurons with expression of KV4.2W362F: Molecular dissection of IA. J. Neurosci. *20*, 5191–5199.

Malinow, R., and Malenka, R.C. (2002). AMPA receptor trafficking and synaptic plasticity. Annu. Rev. Neurosci. *25*, 103–126.

Man, H.Y., Lin, J.W., Ju, W.H., Ahmadian, G., Liu, L., Becker, L.E., Sheng, M., and Wang, Y.T. (2000). Regulation of AMPA receptor-mediated synaptic transmission by clathrin-dependent receptor internalization. Neuron *25*, 649–662.

Ngo-Anh, T.J., Bloodgood, B.L., Lin, M., Sabatini, B.L., Maylie, J., and Adelman, J.P. (2005). SK channels and NMDA receptors form a Ca^{2+}-mediated feedback loop in dendritic spines. Nat. Neurosci. *8*, 642–649.

Nong, Y., Huang, Y.Q., Ju, W., Kalia, L.V., Ahmadian, G., Wang, Y.T., and Salter, M.W. (2003). Glycine binding primes NMDA receptor internalization. Nature *422*, 302–307.

Osten, P., Srivastava, S., Inman, G., Vilim, F., Khatri, L., Lee, L., States, B., Einheber, S., Milner, T., and Hanson, P. (1998). The AMPA receptor GluR2 C terminus can mediate a reversible, ATP-dependent interaction with NSF and α- and β-SNAPs. Neuron *21*, 99–110.

Park, M., Penick, E.C., Edwards, J.G., Kauer, J.A., and Ehlers, M.D. (2004). Recycling endosomes supply AMPA receptors for LTP. Science *305*, 1972–1975.

Passafaro, M., Piech, V., and Sheng, M. (2001). Subunit-specific temporal and spatial patterns of AMPA receptor exocytosis in hippocampal neurons. Nat. Neurosci. *4*, 917–926.

Perez-Otano, I., and Ehlers, M.D. (2005). Homeostatic plasticity and NMDA receptor trafficking. Trends Neurosci. *28*, 229–238.

Ramakers, G.M., and Storm, J.F. (2002). A postsynaptic transient K(+) current modulated by arachidonic acid regulates synaptic integration and threshold for LTP induction in hippocampal pyramidal cells. Proc. Natl. Acad. Sci. USA *99*, 10144–10149.

Shaner, N.C., Campbell, R.E., Steinbach, P.A., Giepmans, B.N., Palmer, A.E., and Tsien, R.Y. (2004). Improved monomeric red, orange and yellow fluorescent proteins derived from Discosoma sp. red fluorescent protein. Nat. Biotechnol. *22*, 1567–1572.

Shi, S.H., Hayashi, Y., Petralia, R.S., Zaman, S.H., Wenthold, R.J., Svoboda, K., and Malinow, R. (1999). Rapid spine delivery and redistribution of AMPA receptors after synaptic NMDA receptor activation. Science *284*, 1811–1816.

Singh, B., Ogiwara, I., Kaneda, M., Tokonami, N., Mazaki, E., Baba, K., Matsuda, K., Inoue, Y., and Yamakawa, K. (2006). A K(v)4.2 truncation mutation in a patient with temporal lobe epilepsy. Neurobiol. Dis. *24*, 245–253.

Snyder, E.M., Philpot, B.D., Huber, K.M., Dong, X., Fallon, J.R., and Bear, M.F. (2001). Internalization of ionotropic glutamate receptors in response to mGluR activation. Nat. Neurosci. *4*, 1079–1085.

Spruston, N., Jaffe, D.B., Williams, S.H., and Johnston, D. (1993). Voltage- and space-clamp errors associated with the measurement of electrotonically remote synaptic events. J. Neurophysiol. *70*, 781–802.

Stell, B.M., and Mody, I. (2002). Receptors with different affinities mediate phasic and tonic GABA(A) conductances in hippocampal neurons. J. Neurosci. *22*, RC223.

Tsaur, M.L., Sheng, M., Lowenstein, D.H., Jan, Y.N., and Jan, L.Y. (1992). Differential expression of K+ channel mRNAs in the rat brain and down-regulation in the hippocampus following seizures. Neuron *8*, 1055–1067.

Zhou, Q., Xiao, M., and Nicoll, R.A. (2001). Contribution of cytoskeleton to the internalization of AMPA receptors. Proc. Natl. Acad. Sci. USA *98*, 1261–1266.